



HAL
open science

Zirconium and hafnium fractionation and distribution of Rare Earth Elements in neutral–alkaline waters: Case study of Lake Van hydrothermal system, Turkey

A. Sasmaz, P. Zuddas, M. Cangemi, D. Piazzese, G. Ozek, M. Venturi, P. Censi

► To cite this version:

A. Sasmaz, P. Zuddas, M. Cangemi, D. Piazzese, G. Ozek, et al.. Zirconium and hafnium fractionation and distribution of Rare Earth Elements in neutral–alkaline waters: Case study of Lake Van hydrothermal system, Turkey. *Journal of Geochemical Exploration*, 2021, 226, pp.106784. 10.1016/j.gexplo.2021.106784 . hal-03251873

HAL Id: hal-03251873

<https://hal.sorbonne-universite.fr/hal-03251873v1>

Submitted on 7 Jun 2021

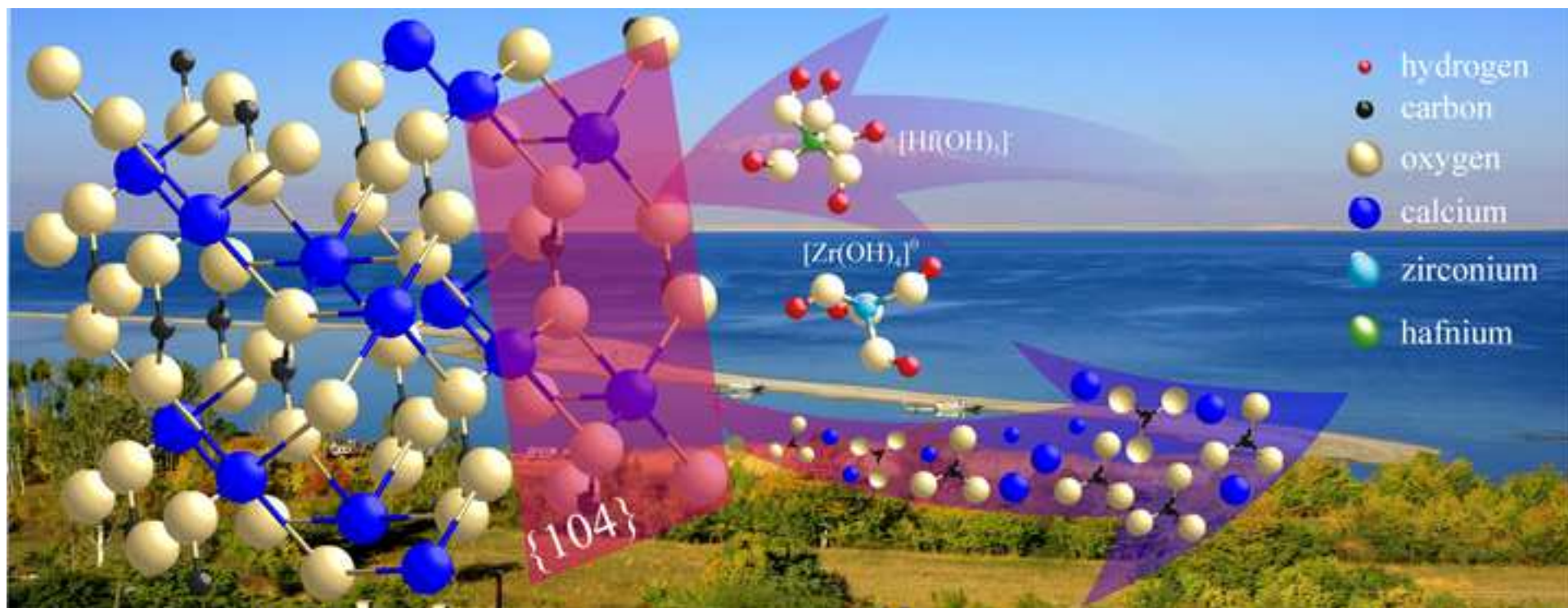
HAL is a multi-disciplinary open access archive for the deposit and dissemination of scientific research documents, whether they are published or not. The documents may come from teaching and research institutions in France or abroad, or from public or private research centers.

L'archive ouverte pluridisciplinaire **HAL**, est destinée au dépôt et à la diffusion de documents scientifiques de niveau recherche, publiés ou non, émanant des établissements d'enseignement et de recherche français ou étrangers, des laboratoires publics ou privés.

Journal of Geochemical Exploration

Zirconium and hafnium fractionation and distribution of rare earth elements in neutral -alkaline waters: Case study of Lake Van hydrothermal system, Turkey --Manuscript Draft--

Manuscript Number:	GEXPLO-D-20-00114
Article Type:	Research Paper
Keywords:	Zr/Hf ratio; REE; Alkaline lakes; Turkey
Corresponding Author:	Paolo Censi University of Palermo: Universita degli Studi di Palermo ITALY
First Author:	Ahmet Sasmaz
Order of Authors:	Ahmet Sasmaz Pierpaolo Zuddas Marianna Cangemi Daniela Piazzese Gulsah Ozek Marco Venturi Paolo Censi
Abstract:	<p>We investigated the distribution of Zr, Hf, and rare earth elements (REE) as the sum of lanthanides plus Y) in the hydrothermal system in the Lake Van area of south-eastern Turkey. This system is characterised by water with variable pH in alkaline conditions resulting from hydrothermal CO₂ upraise and neoformation of calcite minerals in near equilibrium with the interacting waters. Zr, Hf, and REE determinations were carried out for aqueous phases and suspended solids in lake water and surrounding thermal springs. We found that dissolved Hf is partitioned relative to Zr during calcite formation and that such fractionation is a function of the Ca²⁺ activity in warm water. The observed Zr-Hf fractionation is explained by coulombic interactions that occur between suspended solid particles and dissolved phases at the calcite-water interface. There, the surfaces of carbonate minerals demonstrated greater reactivity towards aqueous Hf-bearing species relative to Zr-complexes. This evidence involves a coulombic mechanism of reactivity at the calcite-water interface because Hf complexes are negatively charged while Zr compounds are uncharged. Thus, authigenic calcite can behave as a suitable host for dissolved metal ion species to adsorb on crystal surfaces to remediate waste waters from mine drainage.</p>
Suggested Reviewers:	Thomas H Darrah darrah.24@osu.edu Geochemist with a large experience in REE Rosa Cidu cidur@unica.it Johan Varekamp jvarekamp@wesleyan.edu lake geochemist Yigal Erel yerel@vms.huji.ac.il Trace element geochemist with a large experience in solid-water interface reactions



1 Zirconium and hafnium fractionation and distribution of Rare Earth Elements in neutral–alkaline
2 waters: Case study of Lake Van hydrothermal system, Turkey

3
4 Sasmaz A.¹, Zuddas P.², Cangemi M.³, Piazzese D.³, Ozek G.¹, Venturi M.⁴, Censi P.^{3*}

5
6 1. Firat University, Geological Engineering, 23119, Elazig (Turkey)

7 2. Sorbonne Université, CNRS, METIS - 4, Rue Jussieu, F75005, Paris (France)

8 3. University of Palermo, DiSTeM, Via Archirafi 22, 90123, Palermo (Italy)

9 4. SIDERCEM S.R.L., Via Libero Grassi 7, 93100 Caltanissetta (Italy).

10
11 • corresponding author paolo.censi@unipa.it +393479662844

12
13 Abstract

14 We investigated the distribution of Zr, Hf, and rare earth elements (REE) as the sum of lanthanides
15 plus Y) in the hydrothermal system in the Lake Van area of south-eastern Turkey. This system is
16 characterised by water with variable pH in alkaline conditions resulting from hydrothermal CO₂
17 upraise and neof ormation of calcite minerals in near equilibrium with the interacting waters. Zr, Hf,
18 and REE determinations were carried out for aqueous phases and suspended solids in lake water and
19 surrounding thermal springs. We found that dissolved Hf is partitioned relative to Zr during calcite
20 formation and that such fractionation is a function of the Ca²⁺ activity in warm water. The observed
21 Zr-Hf fractionation is explained by coulombic interactions that occur between suspended solid
22 particles and dissolved phases at the calcite-water interface. There, the surfaces of carbonate
23 minerals demonstrated greater reactivity towards aqueous Hf-bearing species relative to Zr-
24 complexes. This evidence involves a coulombic mechanism of reactivity at the calcite-water
25 interface because Hf complexes are negatively charged while Zr compounds are uncharged. Thus,

26 authigenic calcite can behave as a suitable host for dissolved metal ion species to adsorb on crystal
27 surfaces to remediate waste waters from mine drainage.

28

29 Keywords

30 Zr/Hf ratio; REE; Alkaline lakes; Turkey

31 **1 Introduction**

32 Zirconium, Hf, and REEs are used in specialised technology industries notwithstanding their
33 limited production (Chakhmouradian and Wall, 2012; Jones III et al., 2017). Demand for these
34 elements is high leading an effort by the mineral exploration industry to understand genetic
35 processes and discover new resources. Geochemically, these elements were considered to be
36 ‘immobile’ in subsurface conditions while some works indicate easy water transport under
37 subsurface hydrothermal conditions. Accordingly, REE enrichment has been observed in deposits
38 formed from carbonisation in alkaline environments where Zr concentrations were enriched by a
39 factor of 3 to 4 (Estrade et al., 2015). The behaviour of these strategic elements under surface and
40 subsurface conditions is often neglected because of difficulties in accurate analytical determination
41 at the level of pmol/kg in natural water. In a recent survey, the dissolved Zr/Hf ratio was different
42 from that found in the rock minerals (Censi et al., 2020; Inguaggiato et al., 2015, 2016; Parisi et al.,
43 2017; Tepe and Bau, 2015; Zuddas et al., 2017, 2018) suggesting that the subsurface cycle is
44 important in the accumulation of these elements. In fact, the Zr/Hf molar value in rock minerals was
45 71.4 ± 5.6 which corresponds to the so-called ‘chondritic’ signature (Jochum et al., 1986), while
46 natural water had a wider range of Zr/Hf (Zuddas et al., 2018). The supergene geochemical cycle of
47 Zr and Hf participates in the accumulation and stability of these elements through the process of
48 dissolution and precipitation of the minerals. Because the composition of subsurface and surface
49 waters is often near equilibrium with carbonate minerals like calcite, calcite is expected to play a
50 significant role in the supergene behaviour of these elements. Although carbonates are among the
51 most common minerals in equilibrium with natural water, the formation of neogenic calcite also
52 determined the change in REE distribution observed by Moller and De Lucia (2020) in controlled
53 laboratory investigations. To explain Zr-Hf decoupling during calcite crystallisation and the
54 concurrent behaviour of REEs, we investigated the distribution of these elements in a natural
55 hydrothermal system characterised by the formation of calcite under the neutral and alkaline water
56 system found at Lake Van and characterised by low thermal and lake waters with pH ranging from 6

57 to 10, resulting from a variable CO₂ flux (Degens and Kurtman, 1978; Moller and Bau, 1993). The
58 Lake Van system is characterised by neogenic precipitation in the form of Ca-Mg carbonates
59 (Moller and Bau, 1993).

60 **2 Material and Methods**

61 **2.1 Field sampling**

62 Lake Van is located in south-eastern Turkey (Fig. 1) which formed during the collision
63 between European and Arabian plates. Field study and water sampling were conducted in November
64 2018 and consisted of a 16 samples collected from lake water and thermal springs. Coordinates and
65 geologic units of the collected samples are given in Table 1. Lake water was sampled at a depth of
66 15–20 cm. Physicochemical parameters (pH, redox potential (Eh), temperature, and electrical
67 conductivity) were measured with an Eh oxytrode Pt probe (HamiltonTM) using a standard reference
68 solution buffer at 475±5 mV. Accuracy of determinations was ±10 mV. For the major ion
69 determinations, water samples were filtered in the field through 0.45 µm Millipore® cellulose
70 acetate filters into 50 mL polyethylene bottles and acidified with ultrapure HNO₃. Water samples for
71 trace and rare element analyses were collected in 2,000 mL Nalgene bottles at each sampling site.

72 **2.2 Water analysis and thermodynamic modelling**

73 In the laboratory, samples were filtered (Millipore® manifold filter, 47 mm diameter with a
74 0.45 µm pore size cellulose nitrate membrane), then 5% ultrapure HNO₃ acid solution was added to
75 reach pH ≈ 2. Zirconium, Hf, and REEs in aqueous samples were analysed according to the methods
76 of Raso et al. (2013). Briefly, an excess of FeCl₃ (1%) solution was added to each sample (1 L), and
77 a suitable volume of NH₄OH (25%) solution was added to attain a pH of 8 to induce precipitation of
78 solid Fe(OH)₃. During this process, Zr, Hf, and REEs were held onto the surface of the crystallising
79 solid. To ensure that crystallisation of Fe(OH)₃ was complete, the solution was left in a closed flask
80 for 48–72 h in a stirrer. Next, the iron concentration was measured to assess recovery and was
81 consistently greater than 95%. Precipitated Fe(OH)₃, together with Zr, Hf, and REEs, was collected
82 on a membrane filter (Millipore® manifold filter, 47 mm diameter with 0.45 µm pore size). The

83 solid filtrate was then dissolved in 3 M HCl, and the obtained solution was diluted to 1 M HCl prior
84 to analysis using a Quadrupole-ICP-MS (Agilent 7800 series) with an external calibration procedure.
85 The overall strategy and a detailed evaluation of the analytical errors were reported in Raso et al.
86 (2013). The overall enrichment factor measured for Zr, Hf, and REE concentrations corresponded to
87 66.7.

88 Lanthanum, Ce, and Eu anomalies were calculated using equations 1–3 (Alibo and Nozaki,
89 1999):

$$90 \quad \frac{La}{La^*} = \frac{[La]_n}{3*[Pr]_n + 2*[Nd]_n}, \quad (1)$$

$$91 \quad \frac{Ce}{Ce^*} = \frac{2*[Ce]_n}{[La]_n + [Pr]_n}, \text{ and} \quad (2)$$

$$92 \quad \frac{Eu}{Eu^*} = \frac{2*[Eu]_n}{[Sm]_n + [Gd]_n}, \quad (3)$$

93 where the subscript n indicates shale-normalised elemental concentrations calculated relative to the
94 Post Archean Australian Shale (PAAS, Taylor and McLennan, 1995).

95 All chemicals used during laboratory manipulations were ultrapure grade. Ultrapure water
96 (resistivity of 18.2 MΩ cm or better) was obtained from an Arium® mini system (Sartorius, Italy).
97 Nitric acid 65% (w/w), ammonia solution, and HCl acid were purchased from J.T. Baker chemicals.
98 Working standard solutions of the elements studied were prepared daily by stepwise dilution of
99 standard multi-element stock solutions from DBH, Merck, or CPI International (1,000±5 mg/L) in a
100 1 M HCl medium. All labware was polyethene, polypropylene, or Teflon® and the calibration of all
101 volumetric equipment was verified. Assessment of the analytical precision of Zr, Hf, and REEs was
102 performed on five aliquots (500 mL each) of NASS-6 (seawater certified reference material for trace
103 metals) distributed by the National Research Council of Canada. These certified reference materials
104 were treated as water samples according to the procedure mentioned above and the concentrations
105 obtained were compared with those previously reported by Raso et al. (2013) and Lemaitre et al.
106 (2014). Analysed values are reported in Supplementary Data 1.

107 Thermodynamic modelling of the chemical composition of the water performed was using
108 PHREEQC software and adding additional Lawrence Livermore National Laboratory (LLNL)
109 database (version 3.0.6, Parkhurst and Appelo, 2010).

110 **2.3 Suspended solids**

111 X-ray diffraction investigations were carried out with a Philips PW14 1373 X-ray
112 spectrometer (Cu-K α radiation 2Θ range 10–40°, step size 0.02°, and a 1-min step time). The X-ray
113 spectra were analysed by the Rietveld method (Program DiffraPlus TOPAS®, Version 4.0, Bruker
114 AXS Inc., Karlsruhe, Germany) using parameters for the Rietveld refinement method obtained from
115 the Inorganic Crystal Structure Database (ICSD) program. This method consists of fitting the
116 experimental XRD spectrum to the theoretical spectrum (Young, 1993). Scanning electron
117 microscopy (SEM) of suspended particles was carried out on materials collected after filtration onto
118 cellulose nitrate membranes. Dried solids were mounted on an aluminium stub and gold coated. The
119 SEM analyses were carried out using a LEO 440 SEM equipped with an EDS system OXFORD
120 ISIS Link and Si (Li) PENTAFET detector at the SIDERCEM SRL laboratory (Caltanissetta, Italy).
121 Chemical analyses were carried out by digesting 100 mg of each sample in 10 mL of a 1:1
122 HNO₃:H₂O₂ mixture in a sealed Teflon® TFM bomb using a microwave oven (CEM MARS 5
123 device). After digestion, the TFM bomb was rinsed, and the solution was filtered onto previously
124 acid-cleaned 0.45 μ m Millipore® filters to remove silicate residue. The filtered solution was diluted
125 to 50 mL and stored for chemical analyses.

126 **3 Results and Discussion**

127 **3.1 System description**

128 The concentration of major elements, pH, Eh, electric conductivity, and temperature are
129 reported in the Supplementary Data 2. Water samples had ionic strength ranging from 0.024 to 0.222
130 M in thermal water and between 0.004 and 0.443 M in lake water. Thermal water had pH between
131 5.8 and 7.1 and Eh between 0.013 and 0.172 V, while lake water had pH between 8 and 10 and Eh
132 from -0.288 and 0.012 V. Figure 2a shows that lake water preferentially falls in the field of alkaline

133 elements (only two samples have higher Ca^{2+} and Mg^{2+} concentrations) while thermal water fell
134 between alkaline and Ca^{2+} -rich field (few samples fell in the Mg^{2+} corner).

135 The SEM images of the suspended particulates revealed that suspended particulate matter in
136 lake water consisted of authigenic carbonates associated with biogenic detritus and lithic fragments
137 (Fig. 3a-f), while suspended solids in thermal waters were authigenic carbonates and Fe-rich
138 particles and lithogenic fragments (Fig. 3g-i). Iron-bearing particulates in the samples were often
139 mixed with authigenic calcite and dolomite (see elemental maps in Fig. 3i). The X-ray diffraction
140 analyses confirmed the presence of carbonate minerals identified as calcite and low-Mg calcite
141 representing up to 80% of the authigenic minerals (Table 2). Other phases collected were Fe-
142 oxyhydroxides and detritic silicate particles reaching 10–15% of the total mass.

143 Using the chemical composition of the collected samples, we estimated the saturation state
144 with respect to the mineral in equilibrium and found both lake water and thermal water were
145 saturated or oversaturated with respect to calcite or low-Mg calcite. Some water was also saturated
146 with respect to dolomite and goethite in agreement with the results of the X-ray determinations of
147 the collected suspended matter.

148 **3.2 Zr and Hf behaviour**

149 Zr and Hf concentrations in both aqueous and suspended particulate matter are reported in
150 Supplementary Data 3 and 4, respectively. In the aqueous phase, the concentration of Zr and Hf was
151 not homogenous. Lake waters had Zr concentrations between 79 and 4,958 pmol/L while Hf
152 concentrations fell between 2 and 53 pmol/L, and thermal waters had Zr concentrations between 32
153 and 1.425 pmol/L; whereas Hf concentrations fell between 0.5 and 14 pmol/L. The concentrations of
154 Zr and Hf in thermal waters were 1 to 3 orders of magnitude lower than those found in lake water;
155 however, the concentration of Zr as a function of Hf was linearly correlated with an intercept equal
156 to zero and parametrising a single slope of 90.4 ± 1.7 (Fig. 4a). This value was higher than the Zr/Hf
157 value of 71 ± 5.6 for crustal materials and chondrites (Jochum et al., 1986) indicating that the calcite
158 precipitation fractionates the Zr/Hf ratio in water. In the suspended solids from lake water, Zr

159 concentration ranged from 99.5 to 2,533.2 nmol/kg, whereas Hf fell between 2.6 and 77.1 nmol/kg.
160 Suspended solids from thermal water had Zr concentrations between 20.7 and 346.7 nmol/kg and Hf
161 between 0.6 and 6.8 nmol/kg. Similarly, Zr and Hf in solids collected from thermal water were lower
162 compared to suspended solids found in lake water. Figure 4B shows the concentration of Zr as a
163 function of Hf in neogenic calcite from lake water and describes a linear slope of 33.5 similar to
164 calcite in equilibrium with thermal water where the slope was 37.

165 These results show that the Zr/Hf ratio in water is different from that in crustal rocks and that
166 Hf is preferentially enriched in authigenic carbonate minerals. Preferential enrichment of Hf relative
167 to Zr in newly-formed suspended carbonates was unexpected and may result from processes
168 occurring at the surface-water interface. The calcite-water interface is generally represented by an
169 electric double-layer of weak mineral solubility buffered by CO_3^{2-} ions with the ζ potential of the
170 {104} carbonate surface independent of pH (Herberling et al., 2011). Laboratory measurements
171 indicate the positive surface potential (up to 24 mV) when the Ca^{2+} concentration in solution is
172 between 10^{-2} and 10^{-4} M (Al-Mahrouqui et al., 2017). Byrne (2002) made a critical review of
173 stability constants for Zr and Hf hydroxyl complexes based on the work of Sillen and Martell (1964),
174 Baes and Mesmer (1976), Ekberg et al. (2004), and Brown et al. (2005) and estimated that the most
175 abundant Zr and Hf complexes in aqueous phase were $[\text{Zr}(\text{OH})_4]^0$ and $[\text{Hf}(\text{OH})_5]^-$, respectively
176 (Koschinsky and Hein, 2003). Reporting Zr/Hf ratios as a function of pCa ($\text{pCa} = -\log[\text{Ca}^{2+}]$) (Fig. 5),
177 we found two distinct correlation lines, one for thermal water and one for lake water, suggesting that
178 negatively-charged $[\text{Hf}(\text{OH})_5]^-$ complexes were preferentially scavenged onto {104} positive
179 carbonate surfaces and were, in turn, removed from the aqueous phase. This potential mechanism
180 explains the Zr/Hf fractionation observed during calcite precipitation under pH conditions between 7
181 and 10 and should correspond to the higher binding energy between Hf and {104} calcite surface
182 relative to Zr as estimated by theoretical ab initio calculations (Pinto et al., 2017). Our results
183 support the Zr/Hf fractionation observed by Firdaus et al. (2011, 2018) during Fe-oxyhydroxide
184 formation. Fe-oxyhydroxide was in fact positively charged under weak alkaline conditions

185 (Koschinsky and Hein, 2003). On the contrary, Zr-Hf fractionation did not occur onto surfaces of
186 Mn-oxyhydroxides that were negatively charged at the pH up to acidic values (Tripathy et al., 2001).
187 The Zr-Hf fractionation here observed during calcite formation and interpreted as water-interface
188 interaction is consistent with the Zr-Hf fractionation found in stromatolites (Censi et al., 2015),
189 halite (Censi et al., 2017a, 2020), and other groundwater environments (Censi et al., 2017b;
190 Inguaggiato et al., 2015, 2016).

191 **3.3 REE behaviour**

192 Dissolved REE concentrations in lake water and thermal water in the Lake Van system
193 ranged between 7,135 and 76,140 pmol/L and from 168 to 17,426 pmol/L, respectively
194 (Supplementary Data 3). In lake waters the shale normalised pattern (Fig. 6A) reveals the presence
195 of La positive anomaly as well an ‘ascending’ feature leading to enrichment in heavy REE (HREE,
196 from Ho to Lu) while thermal waters have a single slight medium REE (MREE, from Sm to Dy)
197 enrichment (Fig. 6B). In both types of water, Eu anomalies were 0.3 and 4.8 without evidence of a
198 Ce anomaly ($0.1 \leq \text{Ce}/\text{Ce}^* \leq 1$). The progressive increase of REEs observed in the normalised patterns
199 in these waters may result from the values of the stability constants of di-carbonate and carbonate
200 REE-complex ions (Lee and Byrne, 1993; Liu and Byrne, 1998) potentially producing $[\text{REE}(\text{CO}_3)_2]^-$
201 complexes (Johannesson et al., 1994; Johannesson and Lyon, 1994; Kerrich et al., 2002; Moller and
202 Bau, 1993). Our data showed a higher abundance of La and therefore inconsistent with earlier REE
203 measurements from Van Lake waters (Moller and Bau, 1993). The water level of Lake Van has
204 dropped due to climate change over the last 30 years while the input of lithogenic solids increased.
205 The main difference between the REE distribution recognised in lake Van waters and that reported
206 by Moller and Bau (1993) is the lack of positive Ce anomaly in our samples. This may be caused by
207 a larger dissolution of lithogenic particles typical of continental and coastal waters. The dissolution
208 of lithogenic solids usually provides La enrichment in the aqueous phase that can conceal the
209 concurrent Ce enrichment completely or partially (Censi et al., 2007; Greaves et al., 1999; Grenier et
210 al., 2018).

211 Suspended particulate material collected from the lake and thermal waters had a total
212 concentration of REEs ranging between 508.2 and 835.2 nmol/kg and from 102.3 to 278.5 nmol/kg,
213 respectively (Supplementary Data 4). These values are 3 to 4 orders of magnitude higher than the
214 concentrations found in related waters. The shale-normalised REE patterns of suspended calcites
215 collected in lake waters (Fig. 6c) and thermal waters (Fig. 6d) display positive Ce anomalies ranging
216 from 1.1 to 3.1, an enrichment in MREEs with positive Eu anomalies ($0.8 < \text{Eu}/\text{Eu}^* < 4.2$), and
217 slight progressive depletion of HREEs. Suspended solids from thermal waters showed ‘bulged’ REE
218 patterns (Fig. 6D) while solids from lake waters had flatter patterns (Fig. 6C). The REE distribution
219 in shale-normalised patterns usually show MREE enrichment mainly ruled by crystal-chemical
220 reasons, as demonstrated by the review of distribution coefficient values reported by Moller and De
221 Lucia (2020). In suspended solids from thermal water, the MREE enrichment was more evident than
222 in materials collected from lake water. This evidence is probably justified by the concurrent presence
223 of a detrital fraction in the ‘bulge’ of suspended solids from lake water with a ‘flatter’ shale-like
224 trend in the normalised concentration (Taylor and McLennan, 1988).

225 The behaviour of Y-Ho twin is different in lake and thermal waters. In lakes, Y and Ho
226 concentrations ranged from 3,845 to 62,279 pmol/L and 36 to 686 pmol/L respectively, whereas in
227 thermal springs, Y ranges up to 3,577 pmol/L, whereas Ho fell between 2 and 68 pmol/L. The
228 related Y/Ho ratios spanned from 51 to 111 in lake water and between 53 and 162 in thermal water.
229 These ratios fell between chondritic and super-chondritic values. On the contrary, in carbonates from
230 suspended solids, the Y/Ho ratio ranged from 32.4 to 49.6 in lake water and from 28.6 and 47.8 in
231 thermal water. Then Y/Ho values in suspended solids spanned between slight subchondritic to
232 chondritic values ($\text{Y}/\text{Ho} = 52 \pm 5.1$, Jochum et al., 1986).

233 The role played by the formation of calcite in the distribution of REEs in alkaline waters was
234 highlighted by the super-chondritic value of the Y/Ho ratio. Our study revealed that Ho was 2 to 3
235 orders of magnitude higher than Y during calcite formation causing enrichment. The preferential
236 enrichment of Ho in calcite compared to Y observed in our study may reflect the larger value of the

237 Misono softness parameter of Ho^{3+} relative to Y^{3+} (Thompson et al., 2013) due to the different
238 external electronic configuration of these metal ions (Qu et al., 2009).

239 The different fractionation of these elements found during the formation of calcite also
240 reflects other processes. In thermal water, the intensity of the water-rock interaction may cause
241 MREE enrichment (Fig. 6c). Dissolution of lithogenic rocks may be the source of MREE (Bau,
242 1999; Censi et al., 2019; Greaves et al., 1999; Haley et al., 2004; Inguaggiato et al., 2016; Lin et al.
243 2019) and explain MREE enrichment observed in authigenic hydrothermal carbonates (Jakubowicz
244 et al., 2015; Phan et al., 2019; Wang et al., 2020), phosphates (Censi et al., 2007; Hannigan and
245 Sholkovitz, 2001; Reynard et al., 1999; Zhang et al., 2016), sulphates (Censi et al., 2014; 2018; Kagi
246 et al., 1993; Playà et al., 2007; Toulkeridis et al., 1998), and Fe-oxyhydroxides (Bau, 1999;
247 Davranche et al., 2011).

248 **4 Implications and Conclusions**

249 The results of our investigation of water oversaturated with calcite indicate that calcite plays
250 a crucial role in constraining Zr-Hf fractionation and the geochemical behaviour of REEs in alkaline
251 lake waters. The strong reactivity of positively charged {104} surfaces of calcite coupled with the
252 aqueous Zr and Hf speciation lead to preferential accumulation of Hf in calcite relative to Zr. This
253 indication agrees with the larger affinity of Hf towards solid surfaces relative to Zr already
254 evidenced onto the surfaces of Fe-oxyhydroxides. But the Hf removal onto the carbonate surfaces is
255 ruled by pCa, whereas onto the Fe-oxyhydroxide surfaces is ruled by pH. Therefore, changes of the
256 Zr/Hf ratio in natural waters relative to the chondritic signature indicate that these elements are
257 involved in processes occurring at the interface with crystallising authigenic minerals.

258 Differences in the external electronic configuration of Zr and Hf is similar to that between Y
259 and Ho due to differences in softness/hardness between Zr and Hf and between Y and Ho that, in
260 turn, influence hydrolysis during formation of Zr and Hf hydroxyl complexes. This process could be
261 a crucial aspect of the fractionation of these metal ions during calcite formation. Differences in

262 softness between Y and Ho lead increase stability of Ho-O relative to Y-O bonds on solid surfaces
263 and rule Y-Ho fractionation at the solid-liquid interface.

264 Based on previous researches addressed to the larger Hf affinity relative to Zr towards crystal
265 surfaces of halite, potash salts and Fe-oxyhydroxides, this study contributes to demonstrate that the
266 larger surface reactivity of Hf relative to Zr is a widespread phenomenon through the sedimentary
267 processes. The evidence of this phenomenon is detected measuring the Zr/Hf ratio in natural waters
268 and in authigenic minerals.

269

270 ACKNOWLEDGMENT

271 This research was partially funded by the contracts CORI 2017 (University of Palermo) and CON-
272 0037 funded by the SIDERCEM S.R.L. - University of Palermo Agreement and The Science and
273 Technological Research Council of Turkey (TUBITAK 118Y319).

274

275 REFERENCES

- 276 Al-Mahrouqi, D.A., Vinogradov, J., Jackson, M.D., 2017. Zeta potential of artificial and natural
277 calcite in aqueous solution. *Adv. Colloid. Interface Sci.* 240, 60-76.
- 278 Alibo, D.S., Nozaki, Y., 1999. Rare earth elements in seawater: Particle association, shale-
279 normalization, and Ce oxidation. *Geochim. Cosmochim. Acta* 63, 363-372.
- 280 Baes, C. F., Mesmer R. S. 1976. *The Hydrolysis of Cations*. John Wiley & Sons, Ltd, New York,
281 London, Sydney, Toronto.
- 282 Bau, M., 1999. Scavenging of dissolved yttrium and rare earths by precipitating iron oxyhydroxide:
283 Experimental evidence for Ce oxidation, Y-Ho fractionation, and lanthanide tetrad effect.
284 *Geochim. Cosmochim. Acta* 63, 67–77.
- 285 Brown, P.L., Curti, E., Grambow, B. *Chemical Thermodynamics of Zirconium*, Mompean J. P.,
286 Perrone J. (eds.) NEA Data Bank, OECD 2005, pp 512.
- 287 Byrne, R.H., 2002. Inorganic speciation of dissolved elements in seawater: The influence of pH on
288 concentration ratios. *Geochem. T.* 3, 11-16.
- 289 Censi, P., Cangemi, M., Brusca, L., Madonia, P., Saiano, F., Zuddas, P., 2015. The behaviour of
290 rare-earth elements, Zr and Hf during biologically-mediated deposition of silica-stromatolites and
291 carbonate-rich microbial mats. *Gondwana Res.* 27, 209-215.
- 292 Censi, P., Inguaggiato, C., Chiavetta, S., Schembri, C., Sposito, F., Censi, V. and Zuddas, P. (2017a)
293 The behaviour of zirconium, hafnium and rare earth elements during the crystallisation of halite
294 and other salt minerals. *Chem Geol* 453, 80-91.
- 295 Censi, P., Raso, M., Saiano, F., Zuddas, P., Oliveri, E., 2019. Zr/Hf ratio and REE behaviour: A
296 coupled indication of lithogenic input in marginal basins and deep-sea brines. *Deep-Sea Res. Pt II*
297 164, 216-223.
- 298 Censi, P., Raso, M., Yechieli, Y., Ginat, H., Saiano, F., Zuddas, P., Brusca, L., D'Alessandro, W.,
299 Inguaggiato, C., 2017b. Geochemistry of Zr, Hf, and REE in a wide spectrum of Eh and water

300 composition: the case of Dead Sea Fault system (Israel). *Geochem., Geophys., Geosyst.* 18, 844-
301 857.

302 Censi, P., Saiano, F., Zuddas, P., Nicosia, A., Mazzola, S., Raso, M., 2014. Authigenic phase
303 formation and microbial activity control Zr, Hf, and rare earth element distributions in deep-sea
304 brine sediments. *Biogeosciences* 11, 1125–1136.

305 Censi, P., Sirota, I., Zuddas, P., Lensky, N., Merli, M., Saiano, F., Piazzese, D., Sposito, F.,
306 Venturelli, M., 2020. Trace element fractionation through halite crystallisation. *Geochemical*
307 *mechanisms and environmental implications*, *Sci. Total Environ.* 723, art. 137926

308 Censi, P., Sposito, F., Inguaggiato, C., Zuddas, P., Inguaggiato, S., Venturi, M., 2018. Zr, Hf and
309 REE distribution in river water under different ionic strength conditions. *Sci. Total Environ.* 645,
310 837-853.

311 Censi, P., Sprovieri, M., Saiano, F., Di Geronimo, S.I., Larocca, D., and Placenti, F. (2007). The
312 behaviour of REEs in Thailand's Mae Klong estuary: Suggestions from the Y/Ho ratios and
313 lanthanide tetrad effects. *Estuarine, Coastal and Shelf Science* 71(3-4), 569-579.

314 Chakmouradian, A.R., Wall, F., 2012. Rare earth elements—Minerals, mines, magnets (and more):
315 *Elements* 8, 5, 333–340.

316 Davranche M, Grybos M, Gruau G, Pedrot M, Dia A, Marsac R (2011) Rare earth element patterns:
317 a tool for identifying trace metal sources during wetland soil reduction. *Chem Geol* 284:127–137

318 Degens, E.T., Kurtman, F., Eds. *The Geology of Lake Van*, Min. Res. Explor. Inst. Turkey, Ankara,
319 1978, pp. 158.

320 Ekberg, C., Källvenius, G., Albinsson, Y., Brown, P.L., 2004. Studies on the hydrolytic behavior of
321 zirconium (IV). *J. Solution Chem.* 33, 47-79.

322 Estrade G., Salvi, S., Béziat, D., Williams-Jones, A.E., 2015. The Origin of Skarn-Hosted Rare-
323 Metal Mineralization in the Ambohimirahavavy Alkaline Complex, Madagascar. *Economic*
324 *Geology*, v. 110, pp. 1485–1513.

325 Firdaus, M.L., Mashio, A.S., Obata, H., McAlister, J.A., Orians, K.J., 2018. Distribution of
326 zirconium, hafnium, niobium and tantalum in the North Atlantic Ocean, north-eastern Indian
327 Ocean and its adjacent seas, *Deep-Sea Res. Pt I* 140, 128-135.

328 Firdaus, M.L., Minami, T., Norisuye, K., Sohrin, Y. 2011. Strong elemental fractionation of Zr-Hf
329 and Nb-Ta across the Pacific Ocean. *Nat. Geosci.* 4, 227–230.

330 Greaves, M.J., Elderfield, H., Sholkovitz, E.R., 1999. Aeolian sources of rare earth elements to the
331 Western Pacific Ocean. *Mar. Chem.* 68 (1–2), 31–38.

332 Grenier, M., Garcia-Solsona, E., Lemaitre, N., Trull, T.W., Bouvier, V., Nonnotte, P., Beek, P.,
333 Souhaut, M., Lacan, F., Jeandel, C., 2018. Differentiating lithogenic supplies, water mass
334 transport, and biological processes On and Off the Kerguelen Plateau using rare earth element
335 concentrations and neodymium isotopic compositions. *Frontiers in Marine Science*, 5 (NOV), art.
336 no. 426.

337 Haley, B.A., Klinkhammer, G.P., McManus, J., 2004. Rare earth elements in pore waters of marine
338 sediments. *Geochim. Cosmochim. Acta* 68, 1265–1279. [http://dx.doi.org/10.](http://dx.doi.org/10.1016/j.gca.2003.09.012)
339 [1016/j.gca.2003.09.012](http://dx.doi.org/10.1016/j.gca.2003.09.012).

340 Hannigan, R. E., Sholkovitz E. R., 2001. The development of middle rare earth element enrichments
341 in freshwaters: Weathering of phosphate minerals, *Chem. Geol.*, 175, 495-508.

342 Herberling, F., Trainor, T.P., Lützenkirchen, J., Eng, P., Deneke, M.A., Bosbach, D., 2011. Structure
343 and reactivity of the calcite–water interface. *J. Coll. Inter. Sci.* 354, 843-857.

344 Inguaggiato, C., Censi, P., Zuddas, P., D'Alessandro, W., Brusca, L., Pecoraino, G., Bellomo, S.,
345 2016. Zirconium-hafnium and rare earth element signatures discriminating the effect of
346 atmospheric fallout from hydrothermal input in volcanic lake water. *Chem. Geol.* 433, 1–11.

347 Inguaggiato, C., Censi, P., Zuddas, P., Londono, J.M., Chacon, Z., Alzate, D., Brusca, L.,
348 D'Alessandro, W., 2015. Geochemistry of REE, Zr and Hf in a wide range of pH and water
349 composition: the Nevado del Ruiz volcano-hydrothermal system (Colombia). *Chem. Geol.* 417,
350 125–133.

351 Jakubowicz, M., Dopieralska, J., Belka, Z., 2015. Tracing the composition and origin of fluids at an
352 ancient hydrocarbon seep (Hollard Mound, Middle Devonian, Morocco): A Nd, REE and stable
353 isotope study. *Geochim. Cosmochim. Acta* 156, 50-74.

354 Jochum, K.P., Seufert, H.M., Spettel, B., Palme, H., 1986. The solar-system abundances of Nb, Ta,
355 and Y, and the relative abundances of refractory lithophile elements in differentiated planetary
356 bodies. *Geochim. Cosmochim. Acta* 50, 1173-1183.

357 Johannesson, K.H., Lyons, W.B., 1994. The rare earth element geochemistry of Mono Lake water
358 and the importance of carbonate complexing. *Limnology and Oceanography* 39 (5), pp. 1141-
359 1154.

360 Johannesson, K.H., Lyons, W.B., Bird, D.A., 1994. Rare earth element concentrations and speciation
361 in alkaline lakes from the western U.S.A. *Geophysical Research Letters* 21, 773-776.

362 Jones, J.V., III, Piatak, N.M., and Bedinger, G.M., 2017, Zirconium and hafnium, chap. V of Schulz,
363 K.J., DeYoung, J.H., Jr., Seal, R.R., II, and Bradley, D.C., eds., *Critical mineral resources of the*
364 *United States—Economic and environmental geology and prospects for future supply: U.S.*
365 *Geological Survey Professional Paper* 1802, p. V1– V26, <https://doi.org/10.3133/pp1802V>.

366 Kagi, H., Dohmoto, Y., Takano, S. and Masuda, A., 1993. Tetrad effect in lanthanide partitioning
367 between calcium sulphate crystal and its saturated solution. *Chem. Geol.* 107, 71-82.

368 Kerrich, R., Renaut, R.W., Bonli, T., 2002. Trace-element composition of cherts from alkaline lakes
369 in the east African rift: a probe for ancient counterparts. *Spec. Publ.* 73, 277–298.

370 Koschinsky, A., Hein, J.R., 2003. Uptake of elements from seawater by ferromanganese crusts:
371 Solid-phase associations and seawater speciation. *Mar. Geol.* 198, 331-351.

372 Lee J.H., Byrne R. H. (1993). Complexation of trivalent rare earth elements (Ce, Eu, Gd, Tb, Yb) by
373 carbonate ions. *Geochim. Cosmochim. Acta* 57, 295–302.

374 Lemaitre, N., Bayon, G., Ondréas, H., Caprais, J.C., Freslon, N., Bollinger, C., Rouget M.-L., De
375 Prunelé A., Ruffine L., Olu-Le Roy K., Sarthou G., 2014. Trace element behaviour at cold seeps
376 and the potential export of dissolved iron to the ocean. *Earth Planet. Sci. Lett.* 404, 376-388.

377 Lin, J., Nilges, M.J., Wiens, E., Chen, N., Wang, S., Pan, Y., 2018. Mechanism of Gd³⁺ uptake in
378 gypsum (CaSO₄·2H₂O): Implications for EPR dating, REE recovery and REE behavior.
379 *Geochim. Cosmochim. Acta* 258, 63-78.

380 Liu, X.W., Byrne, R.H., 1998. Comprehensive investigation of yttrium and rare earth element
381 complexation by carbonate ions using ICP-mass spectrometry. *J. Solution Chem.* 27, 803-815.

382 Moller, P., Bau, M. 1993. Rare-earth patterns with positive cerium anomaly in alkaline waters from
383 Lake Van, Turkey. *Earth Planet. Sci Lett.* 117, 671-676.

384 Möller, P., De Lucia, M., 2020. Incorporation of rare earths and yttrium in calcite: A critical re-
385 evaluation. *Aquat. Geochem.*, 26 (2020), pp. 89-117

386 Parisi, M. G., Cammarata, I., Cammarata, M., Censi, V., 2017. Rare earths, zirconium and hafnium
387 distribution in coastal areas: The example of Sabella spallanzanii (Gmelin, 1791). *Chemosphere*
388 185, 268-276.

389 Parkhurst, D.L., Appelo, C.A.J., 2010. User's Guide to PHREEQC (Version 2.17.5) - A Computer
390 program for Speciation, Batch- Reaction, One-Dimensional Transport and Inverse Geochemical
391 Calculations. Available at: [http://www.brr.cr.usgs.gov/projects/
392 GWC_coupled/phreeqc/index.html](http://www.brr.cr.usgs.gov/projects/GWC_coupled/phreeqc/index.html).)

393 Phan, T.T., Hakala, J.A., Lopano, C.L., Sharma S., 2019. Rare earth elements and radiogenic
394 strontium isotopes in carbonate minerals reveal diagenetic influence in shales and limestones in
395 the Appalachian Basin. *Chem. Geol.* 509, 194-212.

396 Pinto, H., Haapasilta, V., Lokhandwala, M., Oberg, S., Foster, A.S., 2017. Adsorption and migration
397 of single metal atoms on the calcite (10.4) surface. *J. Phys.-Condes. Mat.* 29, (13)

398 Playà, E., Cendon, D.I., Trave, A., Chivas, A.R., Garcia, A., 2007. Non-marine evaporites with both
399 inherited marine and continental signatures: The Gulf of Carpentaria, Australia, at similar to 70
400 ka. *Sed. Geol* 201, 267-285.

401 Qu, C.L., Liu, G., Zhao, Y.F., 2009. Experimental study on the fractionation of yttrium from
402 holmium during the coprecipitation with calcium carbonates in seawater solutions. *Geochem. J.*
403 43, 403-414.

404 Raso, M., Censi, P., Saiano, F., 2013. Simultaneous determinations of zirconium, hafnium, yttrium
405 and lanthanides in seawater according to a co-precipitation technique onto iron-hydroxide.
406 *Talanta* 116, 1085–1090.

407 Reynard, B., Lécuyer, C., Grandjean, P., 1999. Crystal-chemical controls on rare-earth element
408 concentrations in fossil biogenic apatites and implications for paleoenvironmental
409 reconstructions. *Chem. Geol.* 155, 233-241.

410 Sillen, L.G., Martell, A.E., 1964. *Stability Constants of Metal–Ion Complexes*, Special Publication
411 17, The Chemical Society, London, pp 754.

412 Taylor, S.R., McLennan, S.M., 1988. The significance of the rare earths in geochemistry and
413 cosmochemistry. *Handbook on the Physics and Chemistry of Rare Earths*, cap. 79, vol. 11, 485-
414 578.

415 Taylor, S.R., McLennan, S.M., 1995. The geochemical evolution of the continental crust. *Rev.*
416 *Geophys.* 33, 241–265.

417 Tepe, N., Bau, M., 2015. Distribution of rare earth elements and other high field strength elements in
418 glacial meltwaters and sediments from the western Greenland Ice Sheet: evidence for different
419 sources of particles and nanoparticles. *Chem. Geol.* 412, 59–68.

420 Thompson, A., Amistadi, M.K., Chadwick, O.A., Chorover, J. Fractionation of yttrium and holmium
421 during basaltic soil weathering. *Geochem. Cosmochim. Acta*, 2013, 119, 18-30.

422 Toulkeridis, T., Podwojewski, P., Clauer, N., 1998. Tracing the source of gypsum in New
423 Caledonian soils by REE contents and S-Sr isotopic compositions. *Chem. Geol.* 145, 61-71.

424 Tripathy, S.S., Kanungo, S.B., Mishra, S.K., 2001. The electrical double layer at hydrous manganese
425 dioxide/electrolyte interface. *J. Colloid Interface Sci.* 241, 112–119.

426 Wang, J.; Chang, J.; Li, C.; Han, Z.; Wang, T.; Han, H., 2020. Significance of Calcite Trace
427 Elements Contents and C-O Isotopic Compositions for Ore-Forming Fluids and Gold Prospecting
428 in the Zhesang Carlin-Like Gold Deposit of Southeastern Yunnan, China. *Minerals* 10, 338.

429 Young, R. *The Rietveld Method*, International Union of Crystallography, Oxford University Press,
430 Oxford, 1993.

431 Zhang, L., Algeo, T.J., Cao, L., Zhao, L., Chen, Z.-Q., Li, Z., 2016. Diagenetic uptake of rare earth
432 elements by conodont apatite. *Palaeogeogr. Palaeoclimatol. Palaeoecol.* 458, 176–197.

433 Zuddas, P., Censi, P., Inguaggiato, C., Sposito, F., 2018 The behaviour of zirconium and hafnium
434 during water-rock interaction. *Appl. Geochem.* 94, 46–52.

435 Zuddas, P., Inguaggiato, C., Censi, P., D'Alessandro, W., 2017. Zr-Hf fractionation during water-
436 rock interaction. *Procedia Earth and Planetary Science* 17, 670-673.

437

438 TABLE CAPTIONS

439 Table 1 - Sampling sites and geographical localisation of studied waters.

440 Table 2 Mineralogical composition of studied suspended particulates in lake waters. Values are
441 given in weight %.

442

443 FIGURE CAPTIONS

444 Figure 1 – Geological sketch map of the studied area.

445 Figure 2 – Major element concentrations analysed in studied waters.

446 Figure 3 – SEM images of suspended solids in studied water samples filtered with membrane
447 porosity 0.45 μm . Fig. 3a, 3b, 3c, and 3d: Different amounts of build-up in suspended solids mixed
448 to authigenic carbonates in lake waters from different sites. Fig. 3e and 3f: Some particulars of well-
449 developed calcite crystals together with biologic remnants in lake waters. Fig. 3g and 3h: Authigenic
450 solids and lithic fragments are suspended in thermal springs. Fig. 3i: Fine-grained Ca-Mg carbonates
451 and Fe-bearing solids in suspended particles from thermal springs. The open square indicates the
452 area where data to depict X-ray Fluorescence maps of Fe, Ca, and Mg were collected.

453 Figure 4 – a: Zr and Hf concentration measured in studied water samples and the linear trend
454 depicted by these analyses. b: Zr and Hf concentration measured in suspended solids in studied
455 water samples. c: Zr and Hf concentration measured in halite crystallising from the Dead Sea brine
456 (data from Censi et al., 2020). Measured Zr and Hf concentrations are compared with the range of
457 Zr/Hf values characteristic of crustal rocks and chondrite ($Zr/Hf = 71 \pm 5.6$, Jochum et al., 1986).

458 Figure 5– Zr/Hf values measured in the dissolved phase of the lake and thermal waters reported
459 towards Ca^{2+} concentration (mol/L) expressed as pCa (see equation 1).

460 Figure 6 – Shale-normalised REE pattern calculated in the dissolved phase of the lake (a) and
461 thermal waters (b). These features are also depicted in terms of MREE/HREE and LREE/MREE
462 ratios (c). Shale-normalised REE pattern calculated for suspended solids in the lake (d) and

463 thermal waters (e). These features are also reported in terms of MREE/HREE and LREE/MREE
464 ratios (f).

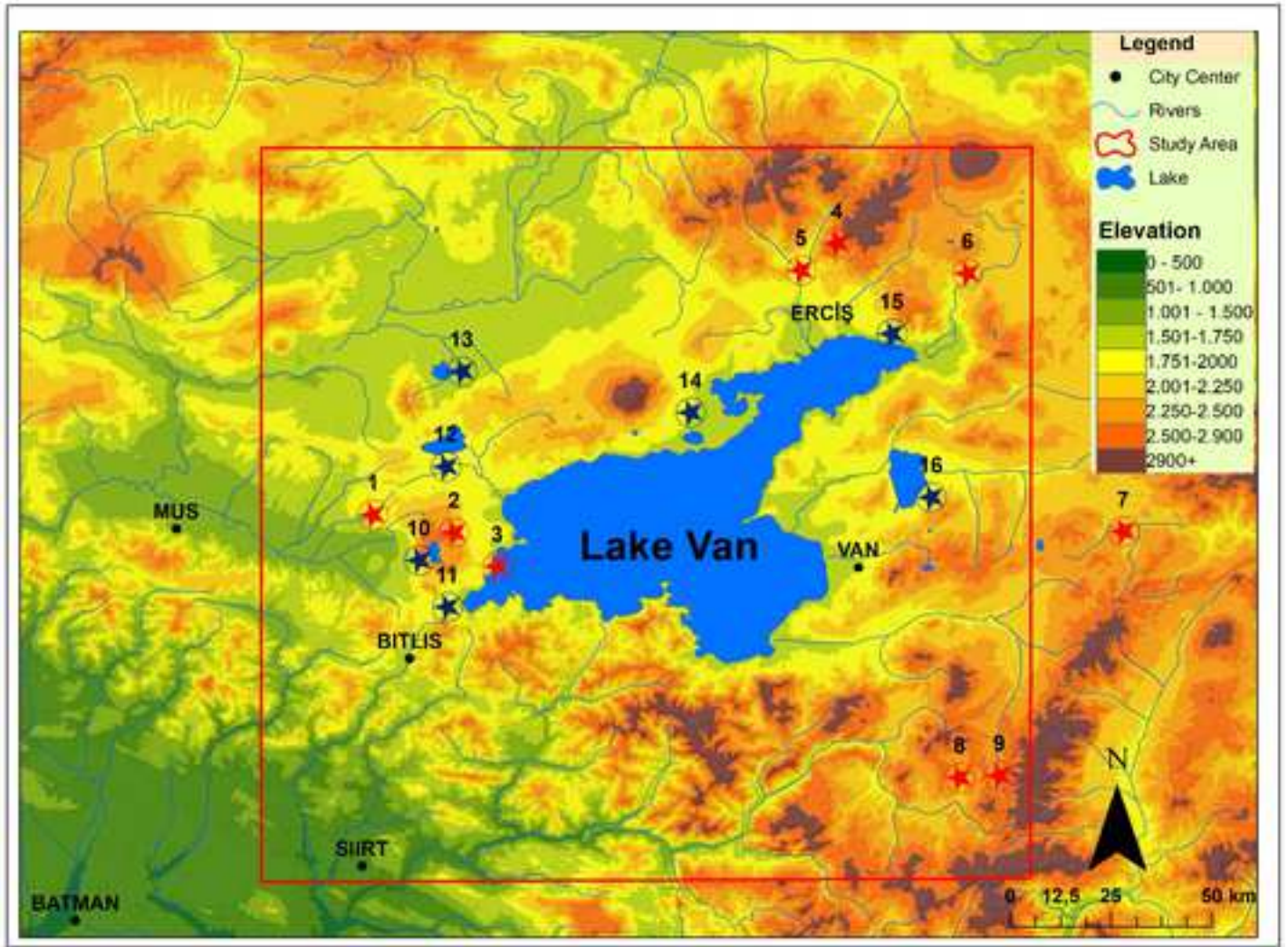


Fig. 1

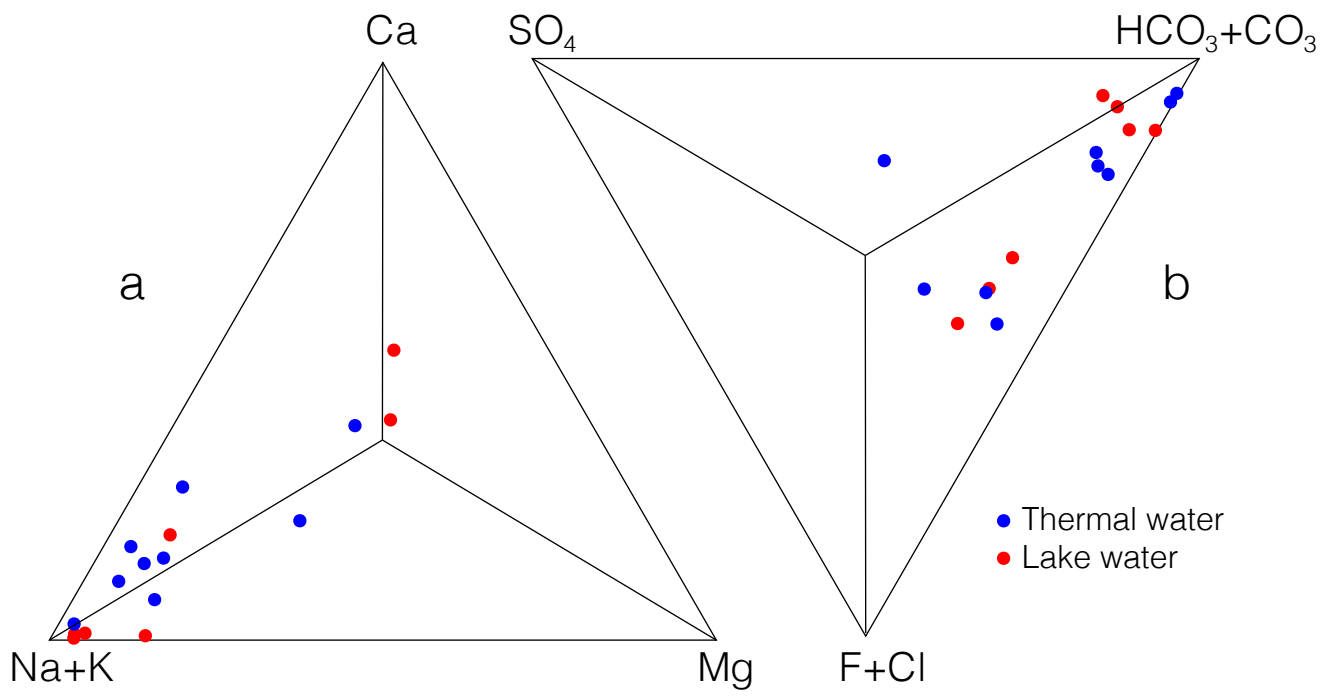


Fig. 2

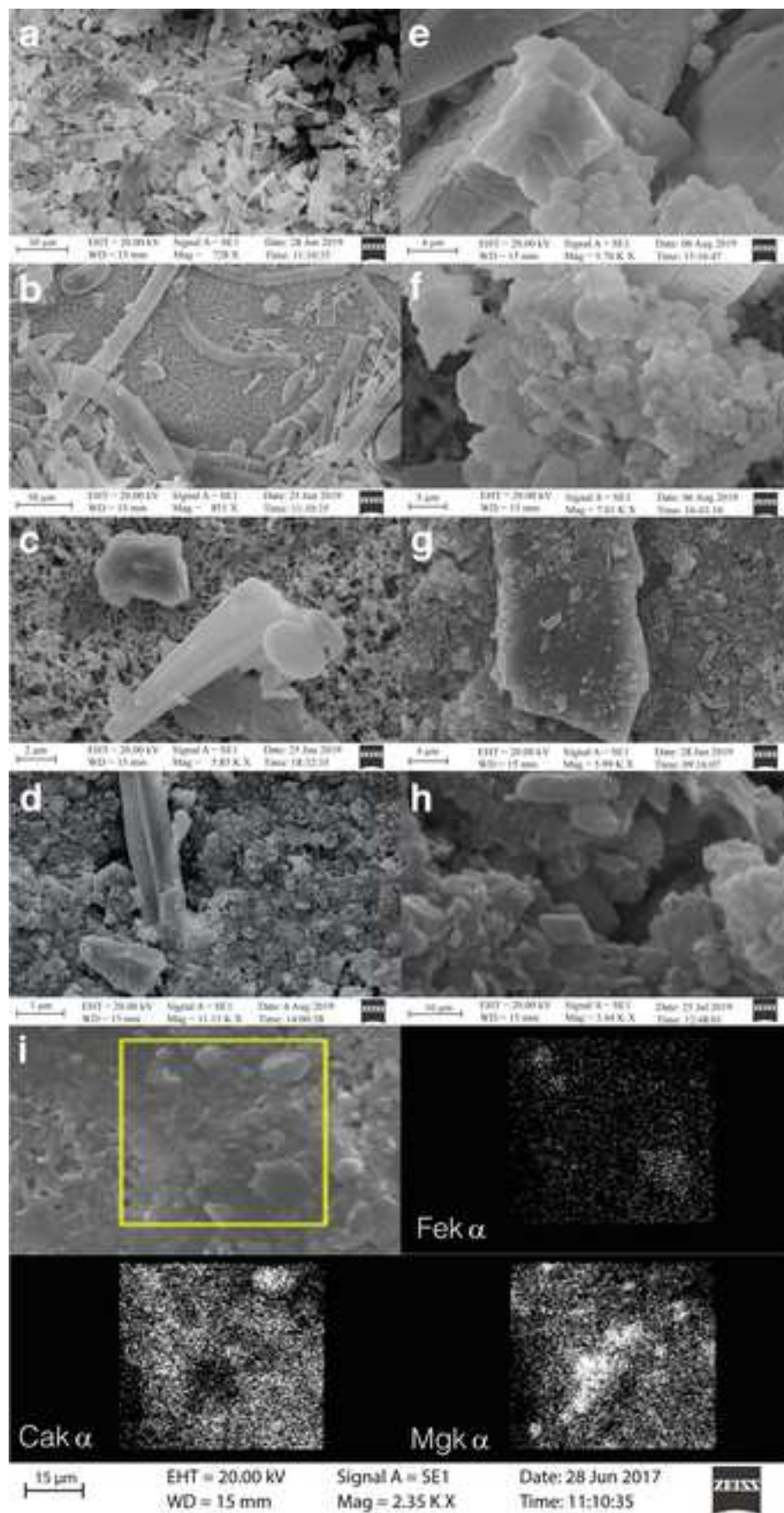


Fig. 3

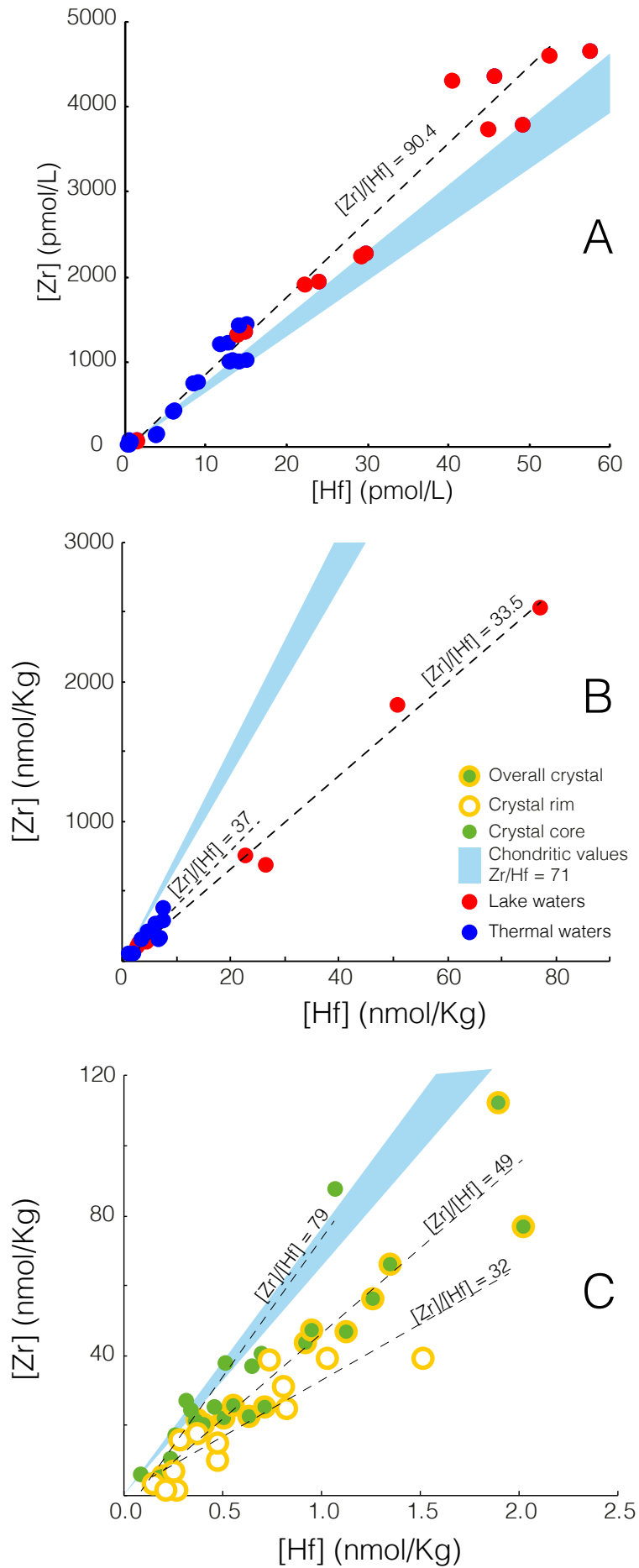


Fig. 4

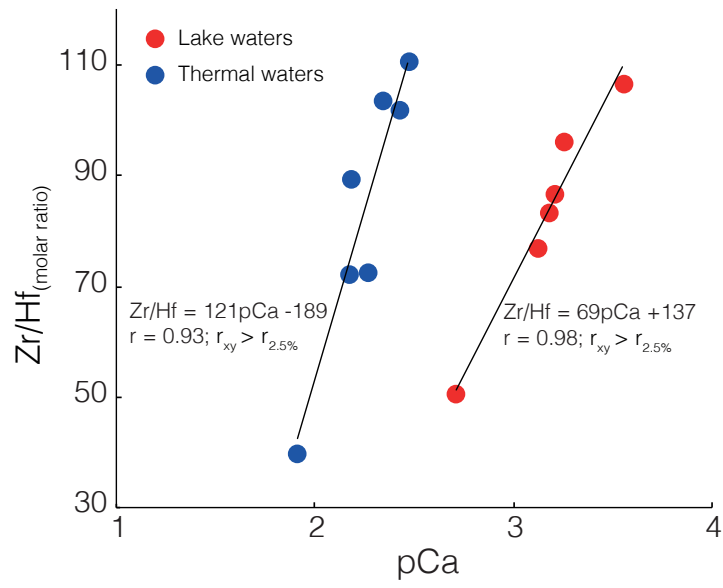


Fig. 5

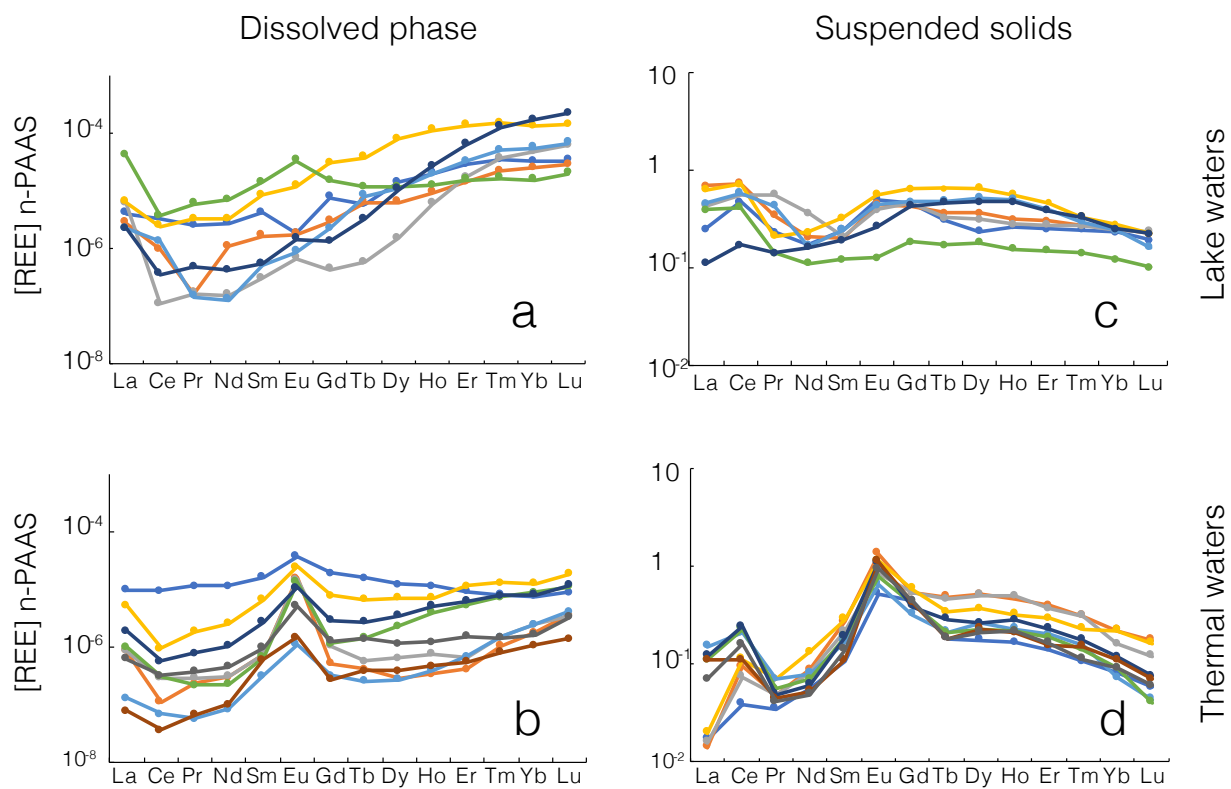


Fig. 6



Click here to access/download

Table

Table 1.pdf





Click here to access/download

Table

Table 2.pdf





UNIVERSITÀ DEGLI STUDI DI PALERMO

Dipartimento di Scienze della Terra e del Mare (DiSTeM)

COD. FISC. 80023730825 ~ P.IVA 00605880822


Palermo, November 14, 2020

CONFLICT OF INTEREST DECLARATION

I subscribed Prof. Paolo Censi, as corresponding author of the paper: “*Zirconium and Hafnium fractionation and distribution of Rare Earth Elements in neutral-alkaline waters: Case study of Lake Van hydrothermal system, Turkey*”

DECLARE

that do not occur conflicts of interest in the submission of the above mentioned paper to *Journal of Geochemical Exploration*.



Click here to access/download
Supplementary Material
Supplementary data.pdf

